PHYSICAL REVIEW B **107**, 125208 (2023)

Level structure of hole two-center complex and related luminescence in semiconductors

I. A. Kokurin[1,2,*] and N. S. Averkiev[1]
[1]*Ioffe Institute, 194021 St. Petersburg, Russia*
[2]*Institute of High Technologies and New Materials, National Research Ogarev Mordovia State University, 430005 Saransk, Russia*

(Received 25 August 2022; revised 15 February 2023; accepted 13 March 2023; published 30 March 2023)

Real semiconductors usually contain both donor and acceptor impurities. A finite compensation degree leads to the possibility of the single carrier to be bounded by two impurity centers. For such an electron complex (near a simple conduction band), the spectral problem resembles the hydrogen molecule ion problem (up to renormalization of the effective mass and dielectric screening). In *p*-type semiconductors, the spectral problem for a single hole in the field of two attracting centers (A_2^- complex) is more complicated due to the complex structure of the valence band. Here such a problem is presented for the case of the hole bounded at two shallow acceptors close to the Γ_8 valence band edge ($\mathrm{A^{III}B^{V}}$ or group IV semiconductors). The multicomponent envelope functions are used to develop quantum chemistrylike approach (molecular orbital method). The variational approach is applied to calculate the level structure of the complex. The states of the complex are classified by the total angular momentum projection onto the intercenter axis and by the parity with respect to the intercenter permutation. The ground state has a total angular momentum projection of ±1/2 and a wave function that is symmetric with respect to the intercenter permutation. The energy levels are found as a function of the intercenter distance. A possible manifestation of A_2^- complexes in acceptor-related luminescence is discussed.

DOI: 10.1103/PhysRevB.107.125208

I. INTRODUCTION

Defects and impurities play a key role in crystals, especially in semiconductors. They can supply mobile charge carriers or vice versa act as traps. In real semiconductors, both donors and acceptors are usually present, i.e., a real semiconductor is partially compensated. Thus, it is necessary to take into account the presence of different charge states of donors and acceptors (at least, neutral and ionized ones) in various phenomena.

A nonzero compensation degree makes possible the optical excitation with the participation of ionized impurities [1,2]: the so-called photoneutralization transition, when the impurity state changes from ionized to neutral. In the case of doping with paramagnetic ions, such an excitation scheme allows direct access to the magnetic moment of the impurity [3,4]. Moreover, the same dopant in the same binary semiconductor can act as both a donor and an acceptor, since it can substitute an atom in the anion or cation sublattice or, in addition, be located in an interstitial site. The presence of different dopant types in a semiconductor crystal and the possible interaction between them can lead to interesting phenomena. In particular, the possibility to control the electron magnetization (or even reverse it) by all-optical means was recently predicted [5].

However, the diversity of impurities is not limited to simple donors and acceptors. More complex compound complexes are also contained in semiconductors. In particular, a neutral donor (acceptor) can capture an additional electron (hole): in this case, one speaks of the so-called D^- and A^+ centers, respectively. In order to obtain such complexes in equilibrium, quantum wells are usually used [6] with joint doping of the well and barrier regions. The complex structure of the valence band leads to a richer level structure of the A^+ center [7,8], especially in quantum wells and/or under the action of external fields [9,10]. On the other hand, there is another possibility in compensated semiconductors: a single charge carrier can be localized by a pair of closely located centers. These complexes should be called D_2^+ and A_2^- for the case of a localized electron and hole, respectively.

In diluted magnetic semiconductors (DMSs), such as GaMnAs, usually the indirect exchange interaction, in the spirit of the Zener or Ruderman-Kittel-Kasuya-Yosida models, is accepted as responsible for ferromagnetism. However, this consideration applies to samples with a manganese content of a few percent, when the exchange is mediated by free holes. At the same time, it is of interest to consider ferromagnetism in DMS in the insulating phase. In this case, an impurity band is not formed, and the indirect exchange occurs due to the overlap of the wave functions of holes localized at acceptors. This corresponds to Mn concentrations up to $10^{19} - 10^{20}$ cm^{-3} [11]. The ferromagnetism on the insulating side of the metal-insulator transition is noticeably weaker and the Curie temperature is lower (units of K). But such samples can find an application, e.g., in superconducting spintronics, more precisely, in ferromagnet/superconductor (F/S) hybrid structures [12]. In this case the low Curie temperature is not so critical, since low temperatures are also required for the existence of superconductivity. A more ideal and well-defined system would consist of a ferromagnetic insulator (FI) instead of a ferromagnetic metal. In the FI/S/FI system, the proximity effect that destroys superconductivity, is limited to the interface because the electron wave function decays in the insulator at an atomic distance [13]. Such a case was discussed

---

[*] ivan.a.kokurin@gmail.com

by de Gennes more than half a century ago [14]. Moreover, the GaMnAs-based structures can be integrated with conventional semiconductor and even silicon electronics.

A consideration of any mechanism of ferromagnetism begins with a study of pair interaction. In this case it is important to consider the interaction of two acceptors. At the same time, it is well known that an attempt to increase the Mn content in GaAs leads to embedding of Mn ions into interstitial sites [11]. In this case, Mn behaves like a double donor, that in turn leads to self-compensation. Thus, to determine the nature of the exchange in insulating GaMnAs, it is important to know the mechanism of interaction not only between two neutral A^0 acceptors (A_2^0 complex), but also between a neutral acceptor A^0 and an ionized A^- one, i.e., A_2^- complex. In this sense, the calculation of the A_2^- energy levels is the first step towards understanding the ferromagnetism in GaMnAs in an insulating state.

The effective mass (including the multiband one) approximation is the main approach that allows us to understand the structure of donors [15–17] and acceptors [18,19], as well as composite complexes [7,8]. The effective mass approximation applied to the D_2^+ complex (near a simple isotropic conduction band) resembles the well-known problem of the hydrogen molecule ion H_2^+ up to renormalization of the effective mass and dielectric screening. In the case of the A_2^- center, the complex structure of the valence band makes the spectral problem nontrivial.

The goal of this work is a theoretical study of the A_2^- complex structure. For this purpose, the multiband effective mass approximation is used. The two-center problem is solved by adopting the well-known in quantum chemistry method of molecular orbitals (MOs) as a linear combination of atomic orbitals (LCAOs) to multicomponent envelope functions. Single-center hole states (corresponding to AOs) [20] are described within the spherical approximation of the Luttinger Hamiltonian [21], which is applicable to describe the valence band of many semiconductors with a diamond or zinc-blende lattice (Ge and $A^{III}B^{V}$).

The paper is organized as follows. In Sec. II the known result for the shallow acceptor A^0 within the spherical approximation is presented, that is the starting point for the A_2^- problem. The spectral problem is solved by means of the variational method. The central-cell correction term (the short-range part of the attracting potential) is also included into the Hamiltonian. Section III is devoted to the spectral problem of the A_2^- complex. The level structure is studied as a function of the intercenter distance. Numerical estimates for the A_2^- complex in GaAs and the possible manifestation of the complex in optical experiments are discussed in Sec. IV. In Sec. V the obtained results are summarized. Calculation details are presented in Appendices A and B.

II. SINGLE ACCEPTOR

The Luttinger Hamiltonian [21] is suitable for describing the Γ_8 valence band states in cubic semiconductors with a wide band gap E_g and a large spin-orbit splitting Δ. For the acceptor problem, there is an additional spherically symmetrical potential $V(r)$. However, the exact solution of the spectral problem is hindered by the cubic symmetry of the Hamiltonian in this case. The way out is to extract the spherically symmetrical part from the initial Hamiltonian. This can be done using an approach based on irreducible spherical tensors [22,23]. The spherical approximation works well for many semiconductors such as Ge, GaAs, and others. Small cubic corrections can be taken into account perturbatively [24]. The spherical approximation is also useful for other problems with spherical symmetry, e.g., for calculating of holes states in spherical quantum dots [25,26].

The ground state ($1S_{3/2}$) of a hole in a spherically symmetrical potential (near the edge of the Γ_8 valence band) is described by a four-component envelope function [27]

$$\Psi_M^{3/2}(r,\theta,\varphi) = 2\sum_{l=0,2}(-1)^{l-3/2+M}R_l(r) \times \sum_{m\mu}\begin{pmatrix} l & 3/2 & 3/2 \\ m & \mu & -M \end{pmatrix} Y_{lm}(\theta,\varphi)X_\mu, \quad (1)$$

which corresponds to the total angular momentum of 3/2 (also Γ_8 symmetry). Here $M = \pm 1/2, \pm 3/2$ is the z projection of the total angular momentum, $Y_{lm}(\theta,\varphi)$ are spherical harmonics, X_μ are eigenvectors of a spin-3/2 matrix J_z, $\mu = \pm 1/2, \pm 3/2$ is the hole spin projection onto the z axis and $\begin{pmatrix} l & 3/2 & 3/2 \\ m & \mu & -M \end{pmatrix}$ are Wigner $3j$-symbols. The orbital angular momentum and its projection are denoted by l and m, respectively. The form of the radial wave functions $R_0(r)$ and $R_2(r)$ depends on the explicit form of the potential $V(r)$.

Wave functions $\Psi_{3/2}^{3/2}$ and $\Psi_{1/2}^{3/2}$ are given by

$$\Psi_{3/2}^{3/2} = \begin{pmatrix} R_0(r)Y_{00}(\theta,\varphi) + \frac{1}{\sqrt{5}}R_2(r)Y_{20}(\theta,\varphi) \\ -\sqrt{\frac{2}{5}}R_2(r)Y_{21}(\theta,\varphi) \\ \sqrt{\frac{2}{5}}R_2(r)Y_{22}(\theta,\varphi) \\ 0 \end{pmatrix},$$

$$\Psi_{1/2}^{3/2} = \begin{pmatrix} \sqrt{\frac{2}{5}}R_2(r)Y_{2,-1}(\theta,\varphi) \\ R_0(r)Y_{00}(\theta,\varphi) - \frac{1}{\sqrt{5}}R_2(r)Y_{20}(\theta,\varphi) \\ 0 \\ \sqrt{\frac{2}{5}}R_2(r)Y_{22}(\theta,\varphi) \end{pmatrix}, \quad (2)$$

and other functions $\Psi_{-3/2}^{3/2}$ and $\Psi_{-1/2}^{3/2}$ are Kramers-conjugated to the above pair (related by the time reversal symmetry).

The spectral problem for the case of an attractive Coulomb potential leads to the following system of differential equations [22,23] for radial wave functions of the ground-state:

$$\begin{pmatrix} \frac{d^2}{dr^2} + \frac{2}{r}\frac{d}{dr} + \frac{2}{r} - E & -\mu_0\left(\frac{d^2}{dr^2} + \frac{5}{r}\frac{d}{dr} + \frac{3}{r^2}\right) \\ -\mu_0\left(\frac{d^2}{dr^2} - \frac{1}{r}\frac{d}{dr}\right) & \frac{d^2}{dr^2} + \frac{2}{r}\frac{d}{dr} - \frac{6}{r^2} + \frac{2}{r} - E \end{pmatrix}\begin{pmatrix} R_0(r) \\ R_2(r) \end{pmatrix} = 0, \quad (3)$$

where $\mu_0 = (6\gamma_3 + 4\gamma_2)/5\gamma_1$ and γ_1, γ_2, γ_3 are the Luttinger parameters [21]. Here, the lengths and energies are in units of the effective Bohr radius and effective Rydberg, respectively:

$$a_B = \frac{\hbar^2\varepsilon\gamma_1}{m_0e^2}, \qquad \mathrm{Ry} = \frac{m_0e^4}{2\hbar^2\varepsilon^2\gamma_1},$$

where m_0 is the free electron mass and ε is the material dielectric constant.

In the general case, this system of equations does not have an analytical solution. Usually it can be solved using the variational method. Here a simple set of trial functions is used [22]

$$f(r) = 2\alpha^{3/2}e^{-\alpha r}, \tag{4a}$$

$$g(r) = \frac{2}{\sqrt{3}}\beta^{5/2}re^{-\beta r}, \tag{4b}$$

since a complex set of functions with multiple variational parameters [23] does not lead to a significant increase in the accuracy of the ground state energy calculation. The difference is about 0.25% for GaAs parameters [28]. Here, the trial functions $f(r)$ and $g(r)$ correspond to $R_0(r)$ and $R_2(r)$, respectively, and α and β are adjustable parameters. It should be noted that these trial functions are normalized independently. This means the appearance of an additional variational parameter c, which takes into account the correct normalization of the multicomponent wave function. Thus, the real trial functions are $cf(r)$ and $dg(r)$ with the additional condition $c^2 + d^2 = 1$ imposed by the normalization.

The system of Eqs. (3), together with trial functions (4a) and (4b), leads to the following expression for the binding energy of the acceptor ground state as a function of the variational parameters and the parameter μ_0, which describes the strength of the spin-orbit coupling:

$$E_0(\alpha, \beta, c; \mu_0) = c^2(-\alpha^2 + 2\alpha) + (1 - c^2)\left(-\frac{7}{3}\beta^2 + \beta\right) - c\sqrt{1 - c^2}\,\frac{16\mu_0\alpha^{5/2}\beta^{5/2}(4\alpha + \beta)}{\sqrt{3}(\alpha + \beta)^4}. \tag{5}$$

In accordance with the results of Ref. [29], the short-range part of the impurity potential (the so-called central-cell correction) $V_{sr}(r)$ can be additionally introduced into the problem using an appropriate potential [30], e.g., a rectangular well of finite depth or Gaussian potential well

$$V_{sr}^{rw}(r) = \begin{cases} -V_0, & r < r_0 \\ 0, & r \geqslant r_0 \end{cases}, \tag{6a}$$

$$V_{sr}^{G}(r) = -V_0 e^{-r^2/r_0^2}, \tag{6b}$$

where r_0 is the characteristic extension of the potential and V_0 is its strength. Finally, to take into account the short-range potential, the following terms should be added into Eq. (5):

$$c^2\langle f|V_{sr}(r)|f\rangle + (1 - c^2)\langle g|V_{sr}(r)|g\rangle. \tag{7}$$

The matrix elements for both types of short-range potential are presented in Appendix A.

The variational minimization of Eq. (5) with the addition of Eq. (7), leads to the dependence of the acceptor binding energy on the parameter μ_0 depicted in Fig. 1. Three cases are considered: (i) a shallow Coulomb acceptor; (ii) an acceptor with an additional short-range potential of the form (6a), and (iii) an acceptor with an additional short-range potential of the form (6b). One can see a significant increase in the ground state binding energy when the short-range potential is taken into account, especially at $\mu_0 > 0.5$.

For the interesting case of GaAs, we have the following set of parameters [31]: $\gamma_1 = 6.85$, $\gamma_2 = 2.10$, $\gamma_3 = 2.90$, and $\varepsilon = 12.4$. This corresponds to the following characteristic values: $\mu_0 = 0.753$, $a_B = 4.47$ nm, and Ry = 13.0 meV. This in turn leads to the following absolute values of the binding energy: 28.1, 57.0, and 59.4 meV, corresponding to a shallow Coulomb center and taking into account two types of short-range potential (6a) and (6b), respectively [32]. In the limit of $\mu_0 = 0$ (the mass ratio of light and heavy holes tends to unity), the equations of system (3) are decoupled. As a result, the binding energy of the shallow A^0 center is simply equal to the effective Rydberg. In this case, the level is insignificantly deepened by the short-range part of the attracting potential.

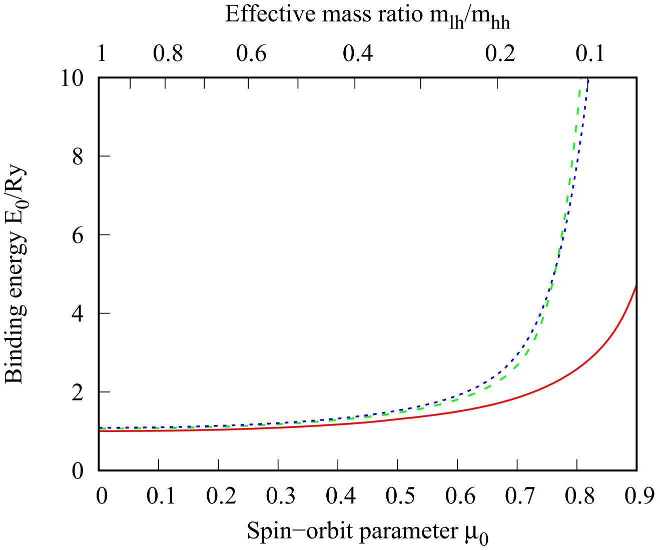

FIG. 1. The binding energy of the ground state of the neutral acceptor A^0 as a function of the parameter μ_0. The red (solid) line corresponds to a shallow Coulomb acceptor, disregarding the short-range potential. The green (dashed) and blue (dotted) lines correspond to taking into account the short-range potential of the form (6a) and (6b), respectively. The top axis shows the dependence of the binding energy on the ratio of the effective masses of light and heavy holes, $m_{lh}/m_{hh} = (1 - \mu_0)/(1 + \mu_0)$. The following dimensionless parameters are used for short-range potentials: $V_0 = 192$ and $r_0 = 0.0626$. In the case of the GaAs band parameters, this corresponds to the dimensional parameters of Ref. [29].

III. SINGLE HOLE IN THE FIELD OF TWO CENTERS

Let us now consider the spectral problem for a hole in the field of two Coulomb centers. Such a system should be called the A_2^- complex. The spectral problem is similar to the problem of the hydrogen molecule ion H_2^+, which is the simplest molecular system. The main difference between H_2^+ and A_2^- is following: the usual term corresponding to the kinetic energy operator should be replaced by the 4×4 Luttinger Hamiltonian [21]. The solution of the problem is significantly complicated by the complex structure of the Γ_8 valence band.

Two-center wave functions (MOs) are composed as a linear combination of single-center wave functions (AOs), i.e., using the standard quantum chemical approach. The explicit form of the AOs is known (see Sec. II). Two centers, denoted A and B, are chosen to be symmetrically located relative to the origin, $\mathbf{R}_{A(B)} = (0, 0, \mp R/2)$, where R is the intercenter distance. The conservation of the total angular momentum projection onto the axis joining the centers A and B (z axis) is implied by the axial symmetry of the problem. This means that MOs can only be composed of AOs with the same M. This leads to the following set of MOs:

$$\Psi^{\pm}_{3/2}(\mathbf{r}) = C^{\pm}_{3/2}\big[\Psi^{3/2}_{3/2}(r_A, \theta_A, \varphi) \pm \Psi^{3/2}_{3/2}(r_B, \theta_B, \varphi)\big], \quad (8a)$$

$$\Psi^{\pm}_{1/2}(\mathbf{r}) = C^{\pm}_{1/2}\big[\Psi^{3/2}_{1/2}(r_A, \theta_A, \varphi) \pm \Psi^{3/2}_{1/2}(r_B, \theta_B, \varphi)\big]. \quad (8b)$$

Here the sign ± denotes the states, that are even (odd) with respect to the intercenter permutations, $A \leftrightarrow B$. The spherical coordinates ($r_A = |\mathbf{r} - \mathbf{R}_A|, \theta_A, \varphi$) and ($r_B = |\mathbf{r} - \mathbf{R}_B|, \theta_B, \varphi$) are introduced: radial distances and polar angles correspond to spherical reference frames with origins at $\mathbf{R}_A$ and $\mathbf{R}_B$, respectively; the azimuthal angle φ is chosen to be the same in both frames of reference due to the coincidence of the polar axes. The states with $M = -3/2, -1/2$ are obtained in a similar way, and their energies are equal to that of states with $M = 3/2, 1/2$, respectively. This is the consequence of the time-reversal symmetry. Thus, four levels with twofold degeneracy are expected. The normalization factors in the wave functions (8a), (8b) are of the standard form

$$C^{\pm}_{M} = \frac{1}{\sqrt{2(1 \pm S_M)}},$$

where S_M is the overlap integral for A- and B- centered AOs with the projection of the total angular momentum M. Details of the calculation of the overlap integrals are presented in Appendix B.

The states with different M are not mixed, that is due to the axial symmetry of the problem. Thus, there are four (according to the number of possible projections M) independent spectral problems. The two-center problem is solved in usual manner [33,34], taking into account the solution of the single-center spectral problem. Moreover, the similar matrix elements appears as in the H_2^+ problem: the overlap integral S, the Coulomb integral J and the resonance integral K. However, the form of these integrals is significantly different, because to calculate these integrals, it is necessary to use multicomponent AOs (2) with trial functions of the form (4a) and (4b).

The energy levels are determined from an equation similar to that of the H_2^+ problem [33,34], but with three variation parameters,

$$E^{\pm}_{M} = -E_0(\alpha, \beta, c; \mu_0) + \frac{2}{R} - \frac{J_M(\alpha, \beta, c) \pm K_M(\alpha, \beta, c)}{1 \pm S_M(\alpha, \beta, c)}. \quad (9)$$

Here $E_0(\alpha, \beta, c; \mu_0)$ is the binding energy of the neutral acceptor A^0 from Eq. (5). The integrals $J_M(\alpha, \beta, c)$ and $K_M(\alpha, \beta, c)$ are found explicitly (see Appendix B). The $2/R$ term corresponds to the "internuclear" repulsion and can be omitted, since it does not affect the order of the energy levels.

The energy levels of the A_2^- complex are found by numerical minimization of the three-parameter variational Eq. (9). The dependence of the energy levels on the intercenter distance R is shown in Fig. 2. The above set of parameters corresponding to GaAs is used in the numerical calculation. The ground state of the A_2^- complex is described by the z projection of the total angular momentum $M = \pm 1/2$. The corresponding wave function is even with respect to the intercenter permutation ($A \leftrightarrow B$), $\Psi^{+}_{\pm 1/2}$. It should be noted that the same structure of the ground state was also found for the case of the deep A_2^- complex described by zero-range potentials [35]: the order of the other levels is the same.

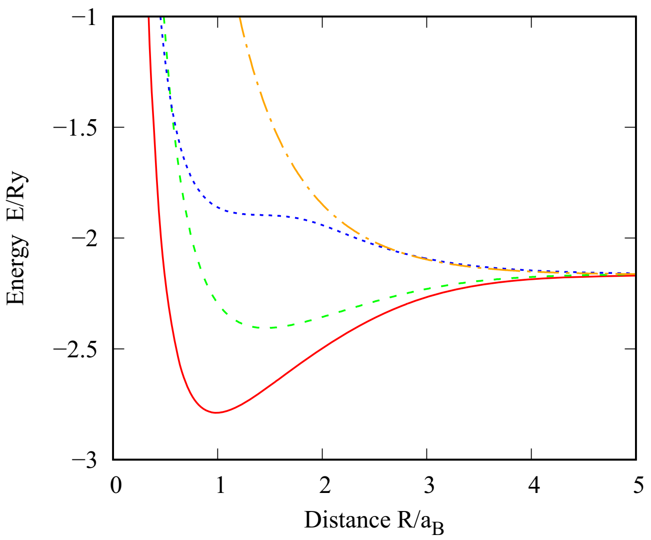

FIG. 2. Energy levels of the A_2^- complex as a function of the intercenter distance R. The band parameters correspond to GaAs (see text). The red (solid) line corresponds to states with $|M| = 1/2$ and a wave function, which is symmetric with respect to the permutation of the centers ($A \leftrightarrow B$), $\Psi^{+}_{\pm 1/2}$. The green (dashed) line corresponds to $|M| = 3/2$ and a wave function, which is antisymmetric relative to $A \leftrightarrow B$, $\Psi^{-}_{\pm 3/2}$. The blue (dotted) line corresponds to $|M| = 3/2$ and the symmetric wave function $\Psi^{+}_{\pm 3/2}$. The orange (dashed-dotted) line corresponds to the states $|M| = 1/2$ with an antisymmetric wave function $\Psi^{-}_{\pm 1/2}$.

The distance corresponding to the maximum binding energy of the ground state (which, by analogy with molecular physics, can be called by "bond length") is about $0.99 a_B$. In the case of GaAs, it is equal to 4.43 nm [36]. The corresponding ionization energy is equal to 2.7882 Ry, which in absolute units is 36.2 meV. In the limit of a long intercenter distance ($R \to \infty$), there is expected result 2.1236 Ry (28.1 meV), which coincides with the A^0 binding energy.

The central-cell correction is not taken into account in the numerical calculations corresponding to Fig. 2. The solution of the spectral problem taking into account the short-range potential (adding the terms $V_{sr}(r_A)$ and $V_{sr}(r_B)$ into the A_2^- Hamiltonian) leads to the following changes in Eq. (9): we have to make replacements, $J_M \to J_M + J^{sr}_M - \Delta E$, $K_M \to K_M + 2K^{sr}_M$, where

$$J^{sr}_M = -\big\langle \Psi^{3/2}_M(r_A, \theta_A, \varphi) \big| V_{sr}(r_B) \big| \Psi^{3/2}_M(r_A, \theta_A, \varphi) \big\rangle,$$

$$K^{sr}_M = -\big\langle \Psi^{3/2}_M(r_A, \theta_A, \varphi) \big| V_{sr}(r_A) \big| \Psi^{3/2}_M(r_B, \theta_B, \varphi) \big\rangle,$$

are the short-range contributions into the Coulomb and resonance integral, respectively. The value of ΔE is determined by Eq. (7). The exact form of J^{sr}_M and K^{sr}_M for potentials (6a) and (6b) is presented in Appendix B. For the parameters of the short-range potential used in the calculation of Fig. 1, simple estimates show that the short-range contributions to the Coulomb and resonance integral are two orders of magnitude smaller than that of the standard Coulomb type. An increase in the short-range contribution is associated with an increase in the strength of the $V_{sr}(r)$ potential, which, in turn, is associated with the need to solve the multiband problem for impurities, which is beyond the scope of this work.

Since the short-range contributions to the Coulomb and resonance integrals are negligible, the energy levels of A_2^- are simply shifted down in energy as a whole. In the first approximation, this shift coincides with the shift of A^0 ground state due to the short-range potential. Thus, any new effects do not appear when the short-range contribution to the impurity potential is taken into account: the energy levels become deeper, but the level order remains the same.

IV. DISCUSSION

We start the discussion with estimates of the accuracy of our variational calculation, estimate the energy of the A_2^- complex in GaAs, consider the conditions under which above complex exists, discuss its possible manifestation in optical experiments, and, finally, examine in details the experimental photoluminescence (PL) data of Ref. [37] taking into account the possible participation of A_2^- complexes.

The accuracy of the our variational calculation can be found in the $\mu_0 \to 0$ limit, which corresponds to a simple band with the scalar effective mass. In this case, there is an exact solution coinciding (up to renormalization of the effective mass and dielectric screening) with the solution for the levels of the hydrogen molecule ion H_2^+. From Fig. 2.2 of Ref. [38] one can see that the maximal error of variational calculation for H_2^+ does not exceed 5%, which takes place at $R \sim 1$ (in atomic units). On the one hand, the error can increase for a complex valence band, and on the other hand, the three-parameter (in contrast to the one-parameter solution in the case of H_2^+) variational procedure used improves the accuracy. Since most A_2^- complexes correspond to $R > 1$, the accuracy can be estimated to be of the same order, i.e., 5% or better.

For the intercenter distance $R = 10$ nm [39] (in GaAs this corresponds to $2.24a_B$) the binding energy of the A_2^- complex is -2.4270 Ry, which is 0.3034Ry (3.94 meV) less than the binding energy of the neutral acceptor A^0. This energy difference corresponds to 45.8 K in temperature units, which means that such A_2^- complexes definitely exist in compensated p-type GaAs at liquid helium (4.2 K). At the same intercenter distance, the energy of the first excited level of the A_2^- complex is 0.1046Ry (1.36 meV or 15.8 K) higher. This means that at 4.2 K the A_2^- complex is in the ground state.

Let us now discuss the possible manifestation of A_2^- complexes in the acceptor-related PL. In partially compensated p-doped semiconductors both A^0 and A_2^- complexes are presented. Both can be additionally formed in the excitation-recombination process. The radiative recombination of a conduction band electron with a hole of the A^0 and A_2^- complex is denoted as $(\mathrm{e}-\mathrm{A}^0)$ and $(\mathrm{e}-\mathrm{A}_2^-)$, respectively. The relative contribution of $(\mathrm{e}-\mathrm{A}^0)$ and $(\mathrm{e}-\mathrm{A}_2^-)$ optical transitions into the total acceptor-related PL line can be changed due to the change in the relative concentrations of A^0 and A_2^- complexes. It might happen, e.g., under conditions of optical excitation (interband or impurity-to-band). The contribution to the PL line from the $(\mathrm{e}-\mathrm{A}_2^-)$ optical transition will have an asymmetric shape, which is due to the spread of A_2^- complexes in the values of the intercenter distances R.

It is supposed that at not too high temperatures, both complexes are in the ground states before recombination. The difference in rates of $(\mathrm{e}-\mathrm{A}^0)$ and $(\mathrm{e}-\mathrm{A}_2^-)$ optical transitions depends not only on concentrations of corresponding complexes. Within the envelope function approximation, it is also determined by a squared electron-hole overlap integral for corresponding transitions. For quasiequilibrium photoexcited electrons in p-type semiconductors the Boltzmann statistics can be utilized. At low temperature the wave vector $\mathbf{k}$ of thermalized electron, which state is described by a plane wave $e^{i\mathbf{kr}}$, is close to zero, and the following conditions are satisfied: $ka_B \ll 1$, $kR \ll 1$. This means, that the electron wave function is approximately constant at the scales of A^0 and A_2^- complexes. This approximation allows us to find the probabilities for both optical transitions exactly. Using Eq. (8) we find that the quantum-mechanical probabilities of electron recombination with the hole in the ground states of A_2^- and A^0 are related as $2/[1 + S_{1/2}(R)]$. Thus, the probability of optical transition is slightly higher for $(\mathrm{e}-\mathrm{A}_2^-)$, which is associated with a stronger spreading of the A_2^- hole wave function.

It should be noted, that the electron-hole overlap integral in the $k = 0$ limit contains contributions from spherically symmetric part of acceptor wave function (1) only, since the spherical harmonics Y_{2m} gives zero after integration in the total solid angle. This feature partly justifies the approximation for $(\mathrm{e}-\mathrm{A}^0)$ transition used by Eagles [1], who did not take into account the multicomponent nature of the acceptor wave function [22,27].

The energy of the quantum emitted during the $(\mathrm{e}-\mathrm{A}_2^-)$ optical transition is on average lower than at $(\mathrm{e}-\mathrm{A}^0)$. An extended low-energy PL tail can be provided by the spread in the binding energy, which, in turn, is due to the spread in the intercenter distances of the A_2^- complexes. Moreover, the decrease in the PL energy is associated not only with an increase in the binding energy of a localized hole, but also with the Coulomb repulsion of ionized centers in the final state. This resembles the donor-acceptor recombination (see, for instance, Ref. [40]), when the attraction of an ionized donor and acceptor in the final state leads to an increase in the transition energy.

The extension of the low-energy PL tail can be estimated simply from the energy of the Coulomb repulsion of two A^- centers located at the minimal intercenter distance $R_{\min}$, which still provides the bound state of the A_2^- complex. From the results of previous section, we have $R_{\min} \sim 0.5a_B$, which leads to a Coulomb energy of the order of the binding energy of the neutral acceptor E_0. Thus, there is a rather extended low-energy PL tail, whose extension is determined by the acceptor binding energy. The width of the high-energy part of the PL band is of the order of the average kinetic energy of the conduction band electron [1], i.e., is determined by the temperature.

An extended low-energy tail of the acceptor-related PL band was first observed about 50 years ago in p-doped GaAs [41]. It should be noted, that only the maximum and the high-energy part of the PL band associated with $(\mathrm{e}-\mathrm{A}^0)$ recombination was described by the simple Eagles theory [1], while the extended low-energy tail has not found a reasonable theoretical interpretation. Attempts to take into account various broadening mechanisms of the $(\mathrm{e}-\mathrm{A}^0)$ transition led to a more regular shape of the central and high-energy part of the line [42]; nevertheless, they were not able to describe an extended low-energy tail.

In low-dimensional structures, acceptor-related PL also takes place. The line shape exhibits the same features as in the bulk. In modern works on the subject, the same feature is manifested [37,43,44], but not discussed. Apparently, the issue was simply forgotten, not finding an explanation after the first experimental observations. These references refer only to GaAs structures, although this phenomenon is general and takes place in other materials. An extended low-energy tail was observed in the acceptor-related PL band of Mn-doped quantum wells [4]. The effect seems to have been enhanced by using a specific excitation scheme (photoneutralization of ionized acceptors) in compensated samples, when the band-to-band optical transitions are excluded from both excitation and recombination processes. It should be noted, that in low-dimensional structures, the influence of the quantum confinement, as well as the width fluctuations, an acceptors position relative to interfaces, etc., can somewhat change and diversify the picture of the phenomenon, but, apparently, the main qualitative features will remain.

Let us discuss the shape of the acceptor-related PL line of Ref. [37] in the light of our consideration. In this work the PL spectra of Be-doped 20 nm wide quantum wells were experimentally studied. Quantum wells with two doping levels are described: 5×10^{10} cm^{-2} and 2.5×10^{12}cm^{-2}, that after recalculation into volume concentrations leads to 2.5×10^{16} cm^{-3} and 1.25×10^{18} cm^{-3}, respectively. Moreover, the δ doping is applied, which in turn means an even higher level of local doping.

The stated binding energy of neutral Be acceptor is 28 meV [37]. This gives the estimate for Bohr radius of 2.5 nm, that is much less than the quantum-well width, i.e., in fact, the acceptors are in the bulk and do not feel quantum confinement, especially taking into account the δ doping. This fact is also confirmed by the so-called fractional dimensionality model [45,46] used in the theoretical fit of absorption and PL lines. This model gives a dimension value of 2.93 [37], which differs little from the bulk value of 3.

In Fig. 9 of Ref. [37] the fit is performed using averaging over a random (Gaussian) distribution, similar to that in Ref. [42]. In this case the central and high-energy part of fitted line is in good agreement with experimental one (especially for the 20 K data). However, the low-energy part shows a long tail that extends even beyond the figure. This behavior coincides with the above-discussed length of this tail on the order of the binding energy of the neutral acceptor.

We ascribe the presence of the discussed tail to the radiative recombination of the conduction band electron with the hole of the A_2^- complex. To confirm this, let us consider how the PL line shape changes with increasing laser excitation intensity, temperature, and doping level. The change in the last parameter is less informative, since there are samples with only two different acceptor concentrations.

The presence of residual donor doping at the level of $10^{14} - 10^{15}$ cm^{-3} is assumed, which is a typical value for epitaxially grown GaAs. This means that for samples with lower levels of p doping, there are about 1–10 percent of A^- ionized centers that can form A_2^- complexes with neutral ones. For heavily doped samples, the fraction of A_2^- is two orders of magnitude lower. If the excitation intensity is low, then the radiative lifetime is long and the A_2^- complexes with a minimal R have time to form. As the excitation intensity increases, the number of photoexcited electrons increases and the radiative lifetime becomes shorter both for the $(\mathrm{e}-\mathrm{A}^0)$ channel and for $(\mathrm{e}-\mathrm{A}_2^-)$ one. In a shorter time, the A_2^- complexes with the smallest intercenter distance R will not be able to form. In addition, the number of A_2^- complexes can be reduced by excitation with photoneutralization (impurity-band transition) [3,4]. Thus, the contribution of the A_2^- complexes with the smallest R to the PL line corresponding to low-energy photon quanta will decrease. Moreover, the contribution of the high-energy part $(\mathrm{e}-\mathrm{A}^0)$ will also increase due to an increase in the number of photoexcited electrons. This means that the discussed low-energy tail will disappear with increasing excitation intensity. The same tendency can be seen in Fig. 2 of Ref. [37].

An increase in temperature leads to the disappearance of the low-energy tail, as can be seen in Fig. 1 of Ref. [37]. Within our model, this is a consequence of the thermal dissociation of two-center complexes $A_2^- \rightarrow A^0 + A^-$ and the growth of the relative $(\mathrm{e}-\mathrm{A}^0)$ contribution. The theoretical fit of Ref. [37] with Gaussian convolution of $(\mathrm{e}-\mathrm{A}^0)$ for two temperatures 3.6 and 20 K (Fig. 9 of Ref. [37]) can also indicate the greater contribution from the $(\mathrm{e}-\mathrm{A}_2^-)$ transition at lower temperature. The authors of Ref. [37] partially reduced the disagreement by increasing the effective electron temperature to 8 K and doubling the Gaussian broadening. However, we believe that the latter manipulation is not fully justified. An additional increase in the electron temperature, say, to 10 K, can lead to a better fit of the high-energy part of the PL line, while the low-energy part can be explained by the contribution of the $(\mathrm{e}-\mathrm{A}_2^-)$ transition.

As for the influence of the acceptor concentration on the shape of the PL line, it is difficult for us to judge the experimental data, since only two samples with different doping levels are presented in Ref. [37]. Two corresponding PL spectra at a sufficiently low excitation intensity are presented in Fig. 3 of Ref. [37]. At the same level of residual donor impurity, the relative amount of A_2^- is higher in samples with lower p doping. Consequently, the relative contribution of the $(\mathrm{e}-\mathrm{A}_2^-)$ transition and, hence, the long-wavelength tail of the PL line should be more pronounced for samples with a lower p-doping level. Figure 3 of Ref. [37] does not contain the theoretical fit of $(\mathrm{e}-\mathrm{A}^0)$-related line (cf., e.g., Fig. 9 of the same work), which makes it difficult to determine the possible contribution of the $(\mathrm{e}-\mathrm{A}_2^-)$ transition. However, in our opinion, the long-wavelength tail is more pronounced in the PL spectrum of the sample with a lower level of p doping.

Detailed qualitative and semiquantitative considerations on the contribution of two-center complexes to acceptor-related PL are presented here, including a comparison with experimental data of Ref. [37]. A detailed microscopic calculation of the corresponding PL line shape will be published elsewhere.[1]

---

[1] The article containing the microscopic calculation of the PL-line shape will be published in Ref. [47].

V. CONCLUSIONS

The spectral problems for A^0 and A_2^- hole complexes in cubic semiconductors are solved. The short-range part of the attracting potential is taken into account. In the case of the A^0 center it leads to a significant increasing in the binding energy, whereas, the levels of the A_2^- complex become deeper as well, but the level order remains unchanged. The dependence of the A_2^--complex energy levels on the intercenter distance is found. It is established, that the ground state of the complex has a projection of the total angular momentum $\pm 1/2$ onto the intercenter axis. The corresponding wave function is symmetric with respect to intercenter permutation, $\Psi^+_{\pm 1/2}$. The A_2^- complex, in addition to a richer level structure, has a higher binding energy than its donor counterpart D_2^+. Estimates are made for the A_2^- complex in GaAs, indicating the existence of the complex at sufficiently high temperatures, above 40 K, even for a shallow complex, without taking into account the short-range part of the impurity potential.

These results are applicable both to stationary complexes, which, as established, can exist in compensated samples, and to quasiequilibrium ones, which arise in p-type crystals under the optical excitation. The possible manifestation of A_2^- complexes in optical experiments is discussed. The qualitative and semiquantitative description of the PL experiment [37] was made taking into account the dependences on three controlled parameters. This makes it possible to speak about the involvement of A_2^- complex in the acceptor-related PL line: in particular, it is responsible for the extended low-energy tail of corresponding line.

Our results can serve as a first step towards considering the A_2^0 complex, which is an acceptor analog of the hydrogen molecule. The MO-like approach used can be adopted to the A_2^0 problem with less computational costs than the recently used Heitler-London-like approach [48]. In the limit of the large intercenter distances, close values of the binding energy obtained by different methods should be expected. The indirect exchange interaction of magnetic impurities mediated by localized holes is another area of theoretical research that can be developed based on our results.

ACKNOWLEDGMENT

We acknowledge financial support from the Russian Science Foundation (Grant No. 22-12-00139).

APPENDIX A: MATRIX ELEMENTS OF SHORT-RANGE POTENTIAL

In this section, the matrix elements of the short-range potentials (6a) and (6b) between the trial functions (4a) and (4b) are presented. Because of θ- and φ-independent functions, the matrix elements contain only radial integration $\langle x|V_{sr}(r)|x\rangle = \int_0^\infty dr r^2 x^2(r) V_{sr}(r)$, with $x(r) = f(r), g(r)$, as well as at the derivation of Eq. (5)

$$\langle f|V_{sr}^{rw}|f\rangle = -V_0\{1 - [1 + 2\alpha r_0 + 2(\alpha r_0)^2]e^{-2\alpha r_0}\}, \tag{A1}$$

$$\langle g|V_{sr}^{rw}|g\rangle = -V_0\big\{1 - \big[1 + 2\beta r_0 + 2(\beta r_0)^2 + \tfrac{4}{3}(\beta r_0)^3 + \tfrac{2}{3}(\beta r_0)^4\big]e^{-2\beta r_0}\big\}, \tag{A2}$$

$$\langle f|V_{sr}^{G}|f\rangle = -\alpha^3 r_0^3 V_0\{-2\alpha r_0 + \sqrt{\pi}e^{(\alpha r_0)^2}[1 + 2(\alpha r_0)^2]\mathrm{erfc}(\alpha r_0)\}, \tag{A3}$$

$$\langle g|V_{sr}^{G}|g\rangle = -\tfrac{1}{6}\beta^5 r_0^5 V_0\{-2\beta r_0[5 + 2(\beta r_0)^2] + \sqrt{\pi}e^{(\beta r_0)^2}[3 + 12(\beta r_0)^2 + 4(\beta r_0)^4]\mathrm{erfc}(\beta r_0)\}, \tag{A4}$$

where $\mathrm{erfc}(x) = \frac{2}{\sqrt{\pi}}\int_x^\infty dt e^{-t^2}$ is the complementary error function.

However, we can use the fact that the characteristic scale of the change in functions $f(r)$ and $g(r)$ is much larger than r_0. This means that the following approximate formula can be used, $\langle x|V_{sr}(r)|x\rangle = x^2(0)\int_0^\infty dr r^2 V_{sr}(r)$. In this approximation $\langle g|V_{sr}^{rw}|g\rangle, \langle g|V_{sr}^{G}|g\rangle \to 0$, while $\langle f|V_{sr}|f\rangle$ has more simple form

$$\langle f|V_{sr}^{rw}|f\rangle = -\tfrac{4}{3}V_0(\alpha r_0)^3, \tag{A5}$$

$$\langle f|V_{sr}^{G}|f\rangle = -\sqrt{\pi}V_0(\alpha r_0)^3. \tag{A6}$$

APPENDIX B: DETAILS OF INTEGRAL CALCULATION

The complex under study has a cylindrical symmetry. However, ellipsoidal coordinates [49] (also known as confocal elliptic coordinates) are more convenient for the theoretical consideration of molecular systems, such as the hydrogen molecule H_2, the molecule ion H_2^+ or the A_2^- complex. Here, these coordinates are used to calculate the overlap integrals, the Coulomb and resonance integrals, which contain multicomponent envelope functions (AOs) of a single hole (2), localized at the centers A and B. In ellipsoidal coordinates there is a triad (μ, ν, φ) and a elementary volume

$$dV = \frac{R^3}{8}(\mu^2 - \nu^2)d\mu d\nu d\varphi$$

with $1 \leqslant \mu < \infty, -1 \leqslant \nu \leqslant 1, 0 \leqslant \varphi \leqslant 2\pi$.

The new variables are related to two sets of spherical coordinates originating at the centers A and B [corresponding sets of spherical coordinates are designated as (r_A, θ_A, φ) and (r_B, θ_B, φ), respectively] by

$$\mu = \frac{1}{R}(r_A + r_B), \qquad \nu = \frac{1}{R}(r_A - r_B).$$

It is also necessary to represent the spherical harmonics centered near A and B in new coordinates (μ, ν, φ). First of all, the expressions for $\cos\theta_{A(B)}$ and $\sin\theta_{A(B)}$ must be written in new variables (using, for example, the cosine theorem)

$$\cos\theta_{A(B)} = \frac{\mu\nu \pm 1}{\mu \pm \nu}, \tag{B1a}$$

$$\sin\theta_{A(B)} = \frac{\sqrt{(\mu^2-1)(1-\nu^2)}}{\mu \pm \nu}. \tag{B1b}$$

It is convenient to extract from the $A(B)$-centered spherical harmonics the terms depending on φ, $Y_{lm}^{A(B)}(\mu,\nu,\varphi) = y_{lm}^{A(B)}(\mu,\nu)\frac{1}{\sqrt{2\pi}}e^{im\varphi}$. Using the above expressions for $\cos\theta_{A(B)}$ and $\sin\theta_{A(B)}$, the following expressions for φ-independent parts of spherical harmonics are found:

$$\begin{aligned}
y_{00}^{A(B)} &= \frac{1}{\sqrt{2}},\\
y_{20}^{A(B)}(\mu,\nu) &= \frac{1}{2}\sqrt{\frac{5}{2}}\left[\frac{3\mu^2\nu^2 \pm 4\mu\nu + 3 - \mu^2 - \nu^2}{(\mu\pm\nu)^2}\right],\\
y_{21}^{A(B)}(\mu,\nu) &= -\frac{\sqrt{15}}{2}\frac{(\mu\nu\pm 1)\sqrt{(\mu^2-1)(1-\nu^2)}}{(\mu\pm\nu)^2},\\
y_{22}^{A(B)}(\mu,\nu) &= \frac{\sqrt{15}}{4}\frac{(\mu^2-1)(1-\nu^2)}{(\mu\pm\nu)^2}.
\end{aligned}$$

Here, standard definitions and phase conventions for spherical harmonics are used (see, for instance, Ref. [50]).

The radial trial wave functions (4a) and (4b) centered near A and B $[f(|\mathbf{r}-\mathbf{R}_{A(B)}|) = f^{A(B)}(\mu,\nu)$ and $g(|\mathbf{r}-\mathbf{R}_{A(B)}|) = g^{A(B)}(\mu,\nu)]$ in ellipsoidal coordinates are given by

$$f^{A(B)}(\mu,\nu) = 2\alpha^{3/2}e^{-\frac{\alpha R}{2}(\mu\pm\nu)}, \tag{B2a}$$

$$g^{A(B)}(\mu,\nu) = \frac{1}{\sqrt{3}}\beta^{5/2}R(\mu\pm\nu)e^{-\frac{\beta R}{2}(\mu\pm\nu)}. \tag{B2b}$$

By analogy with the H_2^+-ion problem, there are three types of integrals: the overlap integral S, the Coulomb integral J and the resonance integral K. For states with $M=\pm3/2$ and $M=\pm1/2$ the corresponding integrals are different. The structure of wave functions (2) with trial functions of the form (B2a) and (B2b) leads to the following general form of integrals:

$$A_M = c^2A^{(1)} \pm c\sqrt{1-c^2}A^{(2)} + (1-c^2)A^{(3)} \tag{B3}$$

with A being S, J or K. The integrals $S^{(i)}$, $J^{(i)}$ and $K^{(i)}$ $(i=1,2,3)$ are calculated below. The upper sign corresponds to $M=3/2$, and the lower sign corresponds to $M=1/2$. The case $\mu_0=0$ corresponds to a simple band and all integrals coincide with their values for the case of the hydrogen molecule ion H_2^+: $S^{(1)}$, $J^{(1)}$ and $K^{(1)}$. The integrals are written as follows: in the integrands the terms containing $f^\xi(\mu,\nu)f^\zeta(\mu,\nu)$ are included in $A^{(1)}$, terms with $f^\xi(\mu,\nu)g^\zeta(\mu,\nu)$ correspond to $A^{(2)}$, and $g^\xi(\mu,\nu)g^\zeta(\mu,\nu)$ is included in $A^{(3)}$. The equality (inequality) of ξ and ζ is determined by a particular type of integral (S, J, or K). The weight factors in Eq. (B3) are included in this form due to the above grouping.

1. Overlap integrals

The three terms constituting overlap integrals $S_M = \langle\Psi_M^{3/2}(\mathbf{r}-\mathbf{R}_A)|\Psi_M^{3/2}(\mathbf{r}-\mathbf{R}_B)\rangle$ are presented here. The first one is given by

$$S^{(1)} = \frac{\alpha^3R^3}{4}\int_1^\infty d\mu e^{-\alpha R\mu}\int_{-1}^1 d\nu(\mu^2-\nu^2) = e^{-\alpha R}\left[1+\alpha R+\frac{1}{3}(\alpha R)^2\right]. \tag{B4}$$

The second term

$$S^{(2)} = \frac{\alpha^{3/2}\beta^{5/2}R^4}{8\sqrt{3}}\int_1^\infty d\mu e^{-\frac{(\alpha+\beta)R\mu}{2}}\int_{-1}^1 d\nu e^{-\frac{(\alpha-\beta)R\nu}{2}}(\mu+\nu)(3\mu^2\nu^2-4\mu\nu-\mu^2-\nu^2+3),$$

is more cumbersome. The result of integration is

$$\begin{aligned}
S^{(2)} = \frac{16\alpha^{5/2}\beta^{5/2}}{\sqrt{3}(\alpha^2-\beta^2)^4R^3}&\{e^{-\beta R}[72+72\beta R-8(\alpha^2-4\beta^2)R^2-8\beta(\alpha^2-\beta^2)R^3+(\alpha^2-\beta^2)^2R^4]\\
&-e^{-\alpha R}[72+72\alpha R+4(7\alpha^2-\beta^2)R^2+4\alpha(\alpha^2-\beta^2)R^3]\}.
\end{aligned} \tag{B5}$$

The third term

$$S^{(3)} = \frac{\beta^5R^5}{48}\int_1^\infty d\mu e^{-\beta R\mu}\int_{-1}^1 d\nu(\mu^4+\nu^4+4\mu^2\nu^2-6\mu^2-6\nu^2+6)$$

after calculation is given by

$$S^{(3)} = e^{-\beta R}\left[1+\beta R+\frac{1}{9}(\beta R)^2-\frac{2}{9}(\beta R)^3+\frac{1}{45}(\beta R)^4\right]. \tag{B6}$$

2. Coulomb integrals

The Coulomb integral corresponds to the attraction energy of the charge density localized near the center $A(B)$ to the center $B(A)$, $J_M = \langle\Psi_M^{3/2}(\mathbf{r}-\mathbf{R}_A)|\frac{2}{|\mathbf{r}-\mathbf{R}_B|}|\Psi_M^{3/2}(\mathbf{r}-\mathbf{R}_A)\rangle$. The first contribution into Eq. (B3) is given by

$$J^{(1)} = \alpha^3R^2\int_1^\infty d\mu e^{-\alpha R\mu}\int_{-1}^1 d\nu(\mu+\nu)e^{-\alpha R\nu} = \frac{2}{R}[1-(1+\alpha R)e^{-2\alpha R}]. \tag{B7}$$

The second term has the form

$$J^{(2)} = \frac{\alpha^{3/2}\beta^{5/2}R^3}{2\sqrt{3}}\int_1^\infty d\mu e^{-\frac{(\alpha+\beta)R}{2}\mu}\int_{-1}^1 d\nu e^{-\frac{(\alpha+\beta)R}{2}\nu}(3\mu^2\nu^2+4\mu\nu+3-\mu^2-\nu^2). \tag{B8}$$

The result is

$$J^{(2)} = \frac{128\sqrt{3}\alpha^{3/2}\beta^{5/2}}{(\alpha+\beta)^6R^3}\left[1-e^{-(\alpha+\beta)R}\sum_{m=0}^{4}\frac{(\alpha R)^m}{m!}\sum_{n=0}^{4-m}\frac{(\beta R)^n}{n!}\right]. \tag{B9}$$

The third term is given by

$$J^{(3)} = \frac{\beta^5R^4}{12}\int_1^\infty d\mu e^{-\beta R\mu}\int_{-1}^1 d\nu(\mu+\nu)^3e^{-\beta R\nu} = \frac{2}{R}\left[1-\left(1+\frac{3}{2}\beta R+(\beta R)^2+\frac{1}{3}(\beta R)^3\right)e^{-2\beta R}\right]. \tag{B10}$$

3. Resonance integrals

The resonance integral corresponds to the attraction energy of "mixed" charge density $\Psi_M^{3/2}(\mathbf{r}-\mathbf{R}_A)\Psi_M^{3/2}(\mathbf{r}-\mathbf{R}_B)$ to each center: $K_M = \langle\Psi_M^{3/2}(\mathbf{r}-\mathbf{R}_A)|\frac{2}{|\mathbf{r}-\mathbf{R}_A|}|\Psi_M^{3/2}(\mathbf{r}-\mathbf{R}_B)\rangle$.

The first contribution into Eq. (B3) is given by

$$K^{(1)} = \alpha^3R^2\int_1^\infty d\mu e^{-\alpha R\mu}\int_{-1}^1 d\nu(\mu-\nu) = 2\alpha e^{-\alpha R}(1+\alpha R). \tag{B11}$$

The second term is

$$K^{(2)} = \frac{\alpha^{3/2}\beta^{5/2}R^3}{2\sqrt{3}}\int_1^\infty d\mu e^{-\frac{(\alpha+\beta)R}{2}\mu}\int_{-1}^1 d\nu e^{-\frac{(\alpha-\beta)R}{2}\nu}(3\mu^2\nu^2-4\mu\nu+3-\mu^2-\nu^2), \tag{B12}$$

and it is calculated in the same manner

$$K^{(2)} = -\frac{128\sqrt{3}\alpha^{3/2}\beta^{5/2}}{(\alpha^2-\beta^2)^3R^3}\left\{e^{-\alpha R}\left[1+\alpha R+\frac{1}{3}(\alpha R)^2\right]-e^{-\beta R}\left[\sum_{n=0}^{4}\frac{(\beta R)^n}{n!}-\frac{1}{6}(\alpha R)^2\sum_{n=0}^{2}\frac{(\beta R)^n}{n!}+\frac{1}{24}(\alpha R)^4\right]\right\}. \tag{B13}$$

The last term is more difficult for calculation

$$K^{(3)} = \frac{\beta^5R^4}{12}\int_1^\infty d\mu e^{-\beta R\mu}\int_{-1}^1 d\nu\frac{6+\mu^4-6\nu^2+\nu^4-6\mu^2+4\mu^2\nu^2}{(\mu+\nu)}. \tag{B14}$$

It is convenient to divide this integral into two parts, $K^{(3)} = K_1^{(3)} + K_2^{(3)}$, using the following relation:

$$\frac{6+\mu^4-6\nu^2+\nu^4-6\mu^2+4\mu^2\nu^2}{(\mu+\nu)} = \nu^3-\mu\nu^2+(5\mu^2-6)\nu+(6\mu-5\mu^3)+6\frac{(1-\mu^2)^2}{(\mu+\nu)}.$$

The first part

$$K_1^{(3)} = \frac{\beta^5R^4}{12}\int_1^\infty d\mu e^{-\beta R\mu}\int_{-1}^1 d\nu[\nu^3-\mu\nu^2+(5\mu^2-6)\nu+(6\mu-5\mu^3)] \tag{B15}$$

is simple in calculation:

$$K_1^{(3)} = -5\beta e^{-\beta R}\left[1+\beta R+\frac{14}{45}(\beta R)^2-\frac{1}{45}(\beta R)^3\right], \tag{B16}$$

while the second one

$$K_2^{(3)} = \frac{\beta^5R^4}{2}\int_1^\infty d\mu(1-\mu^2)^2e^{-\beta R\mu}\int_{-1}^1\frac{d\nu}{(\mu+\nu)} \tag{B17}$$

requires some effort. The inner integral is simple, and after a change of variable and successive integration by parts, we find

$$K_2^{(3)} = 6\frac{e^{-\beta R}}{R}\left\{2(\ln \beta R + \ln 2 + \gamma)\left[1 + \beta R + \frac{1}{3}(\beta R)^2\right] - 3\beta R - (\beta R)^2 + 2e^{2\beta R}\Gamma(0, 2\beta R)\left[1 - \beta R + \frac{1}{3}(\beta R)^2\right]\right\}, \tag{B18}$$

where $\gamma \simeq 0.577216...$ is the Euler-Mascheroni constant, and $\Gamma(a, z) = \int_z^\infty dt t^{a-1} e^{-t}$ is the incomplete Gamma function.

4. Short-range contribution to Coulomb and resonance integrals

Here the calculation of short-range contribution to the Coulomb $J_M^{sr} = -\langle \Psi_M^{3/2}(\mathbf{r} - \mathbf{R}_A)|V_{sr}(|\mathbf{r} - \mathbf{R}_B|)|\Psi_M^{3/2}(\mathbf{r} - \mathbf{R}_A)\rangle$ and resonance $K_M^{sr} = -\langle \Psi_M^{3/2}(\mathbf{r} - \mathbf{R}_A)|V_{sr}(|\mathbf{r} - \mathbf{R}_A|)|\Psi_M^{3/2}(\mathbf{r} - \mathbf{R}_B)\rangle$ integrals is presented. It is convenient to carry out integration in a spherical reference frame centered at the minimum of $V_{sr}(r)$. The same approximation is used here as was done when calculating Eqs. (A5) and (A6). In this case one should simply find the values of $\Psi_M^{3/2}(r, \theta, \varphi)$ at $(R, \pi, 0)$ and $(0, 0, 0)$, then

$$J_{3/2(1/2)}^{sr} = -[R_0(R) \pm R_2(R)]^2 \int_0^\infty dr r^2 V_{sr}(r), \tag{B19}$$

$$K_{3/2(1/2)}^{sr} = -R_0(0)[R_0(R) \pm R_2(R)] \int_0^\infty dr r^2 V_{sr}(r), \tag{B20}$$

where

$$\int_0^\infty dr r^2 V_{sr}^{rw}(r) = -\frac{1}{3} V_0 r_0^3, \quad \int_0^\infty dr r^2 V_{sr}^G(r) = -\frac{\sqrt{\pi}}{4} V_0 r_0^3.$$

For the variational procedure, it is necessary to make the replacements $R_0(r) \to c f(r)$ and $R_2(r) \to \sqrt{1 - c^2} g(r)$ in these equations, which gives the dependence on three variational parameters (α, β, c).

---

[1] D. M. Eagles, J. Phys. Chem. Solids **16**, 76 (1960).

[2] W. P. Dumke, Phys. Rev. **132**, 1998 (1963).

[3] I. A. Kokurin, P. V. Petrov, and N. S. Averkiev, Semiconductors **47**, 1232 (2013).

[4] P. V. Petrov, I. A. Kokurin, Yu. L. Ivanov, N. S. Averkiev, R. P. Campion, B. L. Gallagher, P. M. Koenraad, and A. Yu. Silov, Phys. Rev. B **94**, 085308 (2016).

[5] I. A. Kokurin, A. Yu. Silov, and N. S. Averkiev, Phys. Rev. B **102**, 041202(R) (2020).

[6] D. M. Larsen, Phys. Rev. B **47**, 16333 (1993).

[7] B. L. Gel'mont, A. V. Rodina, and Al. L. Efros, Sov. Phys. Semicond. **24**, 120 (1990).

[8] N. S. Averkiev and A. V. Rodina, Phys. Solid State **35**, 538 (1993).

[9] P. V. Petrov, Yu. L. Ivanov, K. S. Romanov, A. A. Tonkikh, and N. S. Averkiev, Semiconductors **40**, 1071 (2006).

[10] P. V. Petrov, I. A. Kokurin, Yu. L. Ivanov, G. E. Cirlin, V. E. Sedov, and N. S. Averkiev, Phys. Solid State **60**, 339 (2018).

[11] T. Dietl and H. Ohno, Rev. Mod. Phys. **86**, 187 (2014).

[12] J. Linder and J. W. A. Robinson, Nat. Phys. **11**, 307 (2015).

[13] F. S. Bergeret, A. F. Volkov, and K. B. Efetov, Rev. Mod. Phys. **77**, 1321 (2005).

[14] P. G. De Gennes, Phys. Lett. **23**, 10 (1966).

[15] C. Kittel and A. H. Mitchell, Phys. Rev. **96**, 1488 (1954).

[16] W. Kohn and J. M. Luttinger, Phys. Rev. **98**, 915 (1955).

[17] R. A. Faulkner, Phys. Rev. **184**, 713 (1969).

[18] D. Schechter, J. Phys. Chem. Solids **23**, 237 (1962).

[19] K. S. Mendelson and H. M. James, J. Phys. Chem. Solids **25**, 729 (1964).

[20] From now on, the terms "MO" and "AO" are used without quotes, although the corresponding wave functions are not functions of orbital motion only. We hope this will not cause confusion.

[21] J. M. Luttinger, Phys. Rev. **102**, 1030 (1956).

[22] N. O. Lipari and A. Baldereschi, Phys. Rev. Lett. **25**, 1660 (1970).

[23] A. Baldereschi and N. O. Lipari, Phys. Rev. B **8**, 2697 (1973).

[24] A. Baldereschi and N. O. Lipari, Phys. Rev. B **9**, 1525 (1974).

[25] P. C. Sercel and K. J. Vahala, Phys. Rev. B **42**, 3690 (1990).

[26] Al. L. Efros, Phys. Rev. B **46**, 7448 (1992).

[27] B. L. Gel'mont and M. I. D'yakonov, Sov. Phys. Semicond. **5**, 1905 (1972).

[28] M. A. Semina and R. A. Suris, Semiconductors **45**, 917 (2011).

[29] A. K. Bhattacharjee and C. Benoit à la Guillaume, Solid State Commun. **113**, 17 (1999).

[30] The short-range contribution to the acceptor potential can be included in the single-band calculation if the energy distance to other bands is much greater than the binding energy [51]. For an acceptor with binding energy of 60 meV in GaAs, we have $E_0/E_g = 0.06/1.5 = 0.04$ and $E_0/\Delta = 0.06/0.35 = 0.17$, which are both much less than 1. Thus, taking into account the short-range potential in our scheme still keeps the center to be shallow, and there is no need to take into account the contribution of other bands.

[31] R. Winkler, *Spin-Orbit Coupling in Two-Dimensional Electron and Hole Systems* (Springer, Berlin, 2003).

[32] Unfortunately, we have no possibility to provide the direct comparison with the results of Ref. [29], since the parameters used there in the calculation are not specified. It should also be noted that for μ_0 above 0.7, a slight increase in μ_0 leads to a significant increase in the binding energy. Moreover, the use of a lower value of dielectric constant in Ref. [29] was unjustified, and it is possible to significantly increase the binding energy simply by slight refinement of the band parameters.

[33] I. N. Levine, *Quantum Chemistry*, 4th ed. (Prentice Hall, New Jersey, 1991).

[34] P. W. Atkins and R. S. Friedman, *Molecular Quantum Mechanics* (Oxford University Press, New York, 2011).

[35] N. S. Averkiev and S. Yu. Il'inskii, Phys. Solid State **36**, 278 (1994).

[36] However, it should be remembered that the intercenter distance R is a discrete variable, since in order to be an acceptor, an impurity should be placed in a certain position of the crystal lattice. For example, Be in GaAs acts as an acceptor, when it placed in a cation sublattice.

[37] J. Kundrotas, A. Čerškus, G. Valušis, A. Johannessen, E. Johannessen, P. Harrison, and E. H. Linfield, J. Appl. Phys. **107**, 093109 (2010).

[38] J. C. Slater, *Quantum Theory of Molecules and Solids, Vol. 1: Electronic Structure of Molecules* (McGraw-Hill, New York, 1963).

[39] The specific doping level is not discussed here. When estimating the average intercenter distance of the A_2^- complex, including a quasiequilibrium state (e.g., under optical excitation), one should bear in mind the following. A simple estimate of R from the total acceptor concentration is not suitable for A_2^-: The possibility of hole hopping between a neutral and ionized acceptor leads to the formation of A_2^- complexes with a smaller intercenter distance, reducing the total energy of the crystal.

[40] E. W. Williams and H. B. Bebb, Semicond. Semimet. **8**, 321 (1972).

[41] E. W. Williams and H. B. Bebb, J. Phys. Chem. Solids **30**, 1289 (1969).

[42] M. J. S. P. Brasil, A. A. Bernussi, and P. Motisuke, Solid State Commun. **71**, 13 (1989).

[43] H. Ali, Y. Zhang, J. Tang, K. Peng, S. Sun, Y. Sun, F. Song, A. Falak, S. Wu, C. Qian, M. Wang, Z. Zuo, K.-J. Jin, A. M. Sanchez, H. Liu, and X. Xu, Small **14**, 1704429 (2018).

[44] K. Ben Saddik, A. F. Braña, N. López, B. J. García, and S. Fernández-Garrido, J. Cryst. Growth **571**, 126242 (2021).

[45] F. H. Stillinger, J. Math. Phys. **18**, 1224 (1977).

[46] Z. Bak, Phys. Rev. B **68**, 064511 (2003).

[47] I. A. Kokurin and N. S. Averkiev, Bull. Russ. Acad. Sci.: Phys. **87**(6), (2023).

[48] A. C. Durst, K. E. Castoria, and R. N. Bhatt, Phys. Rev. B **96**, 155208 (2017).

[49] G. A. Korn and T. M. Korn, *Mathematical Handbook for Scientists and Engineers: Definitions, Theorems, and Formulas for Reference and Review* (McGraw-Hill, New York, 1968).

[50] D. A. Varshalovich, A. N. Moskalev, and V. K. Khersonskii, *Quantum Theory of Angular Momentum* (World Scientific, Singapore, 1988).

[51] G. L. Bir and G. E. Pikus, *Symmetry and Strain-induced Effects in Semiconductors* (Wiley, New York, 1974).